Journal of Alloys and Compounds 509 (2011) 3347–3352

Contents lists available at ScienceDirect

Journal of Alloys and Compounds

journal homepage: www.elsevier.com/locate/jallcom

Dependence of lattice distortion of monoclinic phase on film thickness in $Pb(Zr_{0.58}Ti_{0.42})O_3$ thin films

J.N. Wang, L.D. Wang, W.L. Li, W.D. Fei*

State Key Laboratory of Welding Production Technology, School of Materials Science and Engineering, Harbin Institute of Technology, Harbin 150001, PR China

ARTICLE INFO

Article history:
Received 4 November 2010
Received in revised form 3 December 2010
Accepted 8 December 2010
Available online 15 December 2010

Keywords:
$Pb(Zr_{1-x}Ti_x)O_3$ thin films
Lattice distortion
Film thickness
Texture

ABSTRACT

In this paper, the chosen composition of PZT film falls in rhombohedral phase region and the dependence of lattice distortion on film thickness in sol–gel derived $Pb(Zr_{0.58}Ti_{0.42})O_3$ thin films was systematically investigated. The results confirm that the $Pb(Zr_{0.58}Ti_{0.42})O_3$ films have monoclinic phase even though the composition falls in the rhombohedral phase region. The mixed textures of (1 0 0) and (1 1 1) occur in the PZT films. In the case of mixed textures, a method using ψ-scan XRD to characterize the phase type of $Pb(Zr_{0.58}Ti_{0.42})O_3$ film is presented. It is found that the phase type of (1 0 0)-oriented grains is M_A phase, and that of (1 1 1)-oriented grains is M_B phase. Moreover, the lattice constants of both M_A and M_B phases are sensitive to the film thickness. The lattice distortion of monoclinic phase becomes smaller as film thickness increases.

1. Introduction

$Pb(Zr_{1-x}Ti_x)O_3$ (PZT) thin film has been widely used in many applications, such as actuators, sensors, and microelectromechanical systems (MEMS), because of its giant piezoelectric [1–3]. The PZT phase diagram extensively accepted was proposed by Jaffe et al. [4] in 1971. In the phase diagram, the morphotropic phase boundary (MPB) apparently separates the tetragonal phase (T phase) and the rhombohedral phase (R phase) regions. In 1999, Noheda et al. [5] firstly reported the low symmetrical monoclinic phase (M phase) with the space group of *Cm* near MPB. The crystalline symmetry group of M phase is the subgroup of both T phase and R phase. Therefore, the phase transition between R phase and T phase becomes acceptable from the viewpoint of crystalline symmetry [6–9]. Furthermore, the M phase has been considered to be the origin of the giant piezoelectric properties of PZT ceramics with the composition in the vicinity of MPB owing to the symmetry-allowed rotation of the polarization direction of M phase [1,10–12]. Later on, a new PZT phase diagram including M phase was built based on the synchrotron radiation X-ray diffraction (XRD) results, as shown in Fig. 1 [13]. In this new diagram, there is a new dash line (corresponding to $x \approx 0.455$) implying that the Zr-rich side boundary between R phase region and M-included region is still controversial. Yokota et al. [14] reported that PZT powders included the mixed phases (R + M) when $0.08 \leq x \leq 0.4$. Pandey et al. [15] claimed that the single M phase with the space group of *Cc* was found within the R phase region in the phase diagram proposed by Jaffe et al. [4]. Singh et al. [16] found that only M phase was involved in PZT in the case of $0.40 \leq x \leq 0.475$.

Till now, the M phase lattice constants quite differ in the various literatures [13,17–22], as listed in Table 1. These differences were normally ascribed to the differences in sample preparation methods [14]. As well known, the lattice constants are highly dependent of interplanar spacing (d), and residual stress will cause the change of interplanar spacing. Therefore, the residual stress plays the key role in determining lattice constants. For PZT thin films, the film thickness is highly related to the residual stress. However, few reports study the dependence of the lattice constants and the phase transition on film thickness, i.e. lattice distortion of monoclinic phase and R → M phase transition in PZT thin films.

In this study, $Pb(Zr_{0.58}Ti_{0.42})O_3$ (PZT58/42) thin films (here the composition locates in R phase region) were deposited by sol–gel routine. We systematically studied the lattice distortion of monoclinic phase by changing the thickness of PZT thin films.

2. Experimental procedure

PZT58/42 films were prepared on $Pt/Ti/SiO_2/Si$ substrates through sol–gel technology. Lead acetate trihydrate, zirconium *n* propoxide and titanium isopropoxide were used as the raw materials and 2-methoxyethanol [$2\text{-}CH_3OCH_2CH_2OH$] was used as the solvent. The 10 mol% excessive Pb in precursor was added to compensate for the Pb volatility during high temperature annealing. The PZT precursor was firstly spin-coated on the substrate at the spinning rate of 4000 rpm, and then the spin-coated film was pyrolyzed at 500 °C on a hot plate for 2 min. The process was repeated for several times to obtain the desired film thickness. Finally, the PZT58/42 films were annealed at 650 °C for 3 min through rapid thermal annealing technique in the O_2 ambient.

* Corresponding author. Tel.: +86 451 86413908; fax: +86 451 86413908.
E-mail address: wdfei@hit.edu.cn (W.D. Fei).

0925-8388/$ – see front matter © 2010 Elsevier B.V. All rights reserved.
doi:10.1016/j.jallcom.2010.12.061

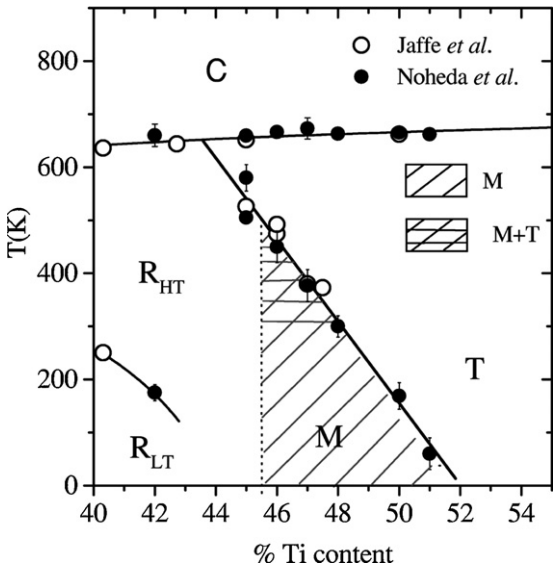

Fig. 1. PZT phase diagram around the MPB proposed by Noheda et al. [13] in 2000.

The XRD analysis of the films was carried out on a Philips X'Pert diffractometer with Cu Kα radiation operated at 40 kV and 40 mA. The θ–2θ scans were conducted at different tilt angles, ψ, where ψ is the angle of the scattering vector of X-ray to the normal direction of the film. Obviously, the normal θ–2θ scan is the case of $\psi = 0^\circ$. The surface and cross-section morphologies were examined by a Hitachi S-4800 scanning electron microscope (SEM). The Raman spectral excitation was provided by an Ar-ion laser with the wave length of 458 nm. The scattered light was analyzed with a Jobin Yvon HR800 spectrometer.

3. Results

3.1. Microstructure and orientations

Typical image of the surface morphology of PZT58/42 film as shown in Fig. 2(a) indicates that the surface of PZT film is dense without any porosity. The cross-section morphology (Fig. 2b) of PZT58/42 film reveals the column grain microstructure. Fig. 3 shows θ–2θ scan XRD curves at $\psi = 0^\circ$. To simplify, the PZT58/42 film diffraction peaks are indexed using pseudo cubic coordinate system, which is denoted by subscript 'C'. Indexing of Fig. 3 confirms that only perovskite phase (without any secondary phase) exists in PZT58/42 films. Besides, only $1\,0\,0_C$, $1\,1\,1_C$ and $2\,0\,0_C$ diffraction peaks are visible, indicative of possibly mixed texture of (1 0 0) and (1 1 1).

In order to determine the textures of PZT58/42 films, ω-scans for (1 1 1) and (2 0 0) diffractions were conducted [23], and the results are shown in Fig. 4. All of the peak positions locate approximately at the Bragg angle of corresponding diffraction planes. This confirms that the PZT58/42 films exhibit (1 1 1) and (1 0 0) mixed textures. Furthermore, the full widths at half maximum (FWHM) of all ω-scan curves are less than 7°, which indicates that the PZT58/42 films contain highly preferential orientations of (1 1 1) and (1 0 0). [23]

Table 1
Lattice constants of M phases reported by different literatures.

x	a (Å)	b (Å)	c (Å)	β (°)	Ref.
0.48	5.7520	5.7431	4.0912	90.48	[17]
	5.7082	5.7078	4.14144	90.199	[18]
	5.71291	5.70725	4.14355	90.1993	[19]
0.47	5.720	5.715	4.142	90.22	[13]
	5.7244	5.7165	4.1279	90.289	[18]
	5.719	5.7785	4.1098	90.64	[20]
0.46	5.754	5.731	4.103	90.47	[13]
	5.74846	5.73094	4.10936	90.426	[21]
	5.744	5.73	4.121	90.431	[22]

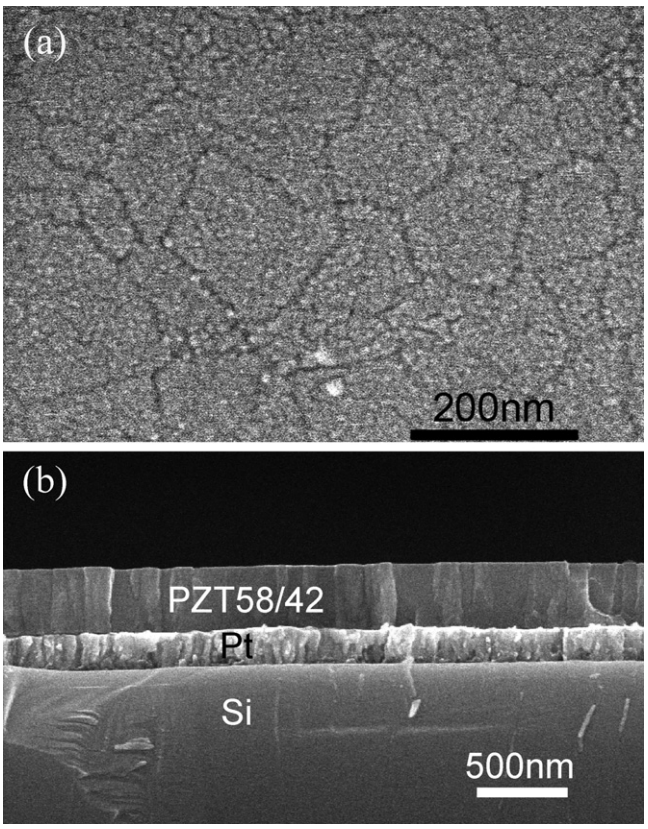

Fig. 2. Surface (a) and the cross section (b) morphologies of PZT58/42 film with the thickness of 350 nm.

3.2. XRD method to analyze the crystal structures for different oriented grains

Generally speaking, for a given grain, the residual stress components in crystalline coordinates are strongly related to its orientation, which would result in different residual stress state in different oriented grains. Therefore, in terms of thin film, it is very difficult to directly use Rietveld refinement in a θ–2θ scan XRD curve because different peaks may belong to different oriented grains. In order to analyze the phase composition with a given orientation, the XRD peaks used must belong to the grains

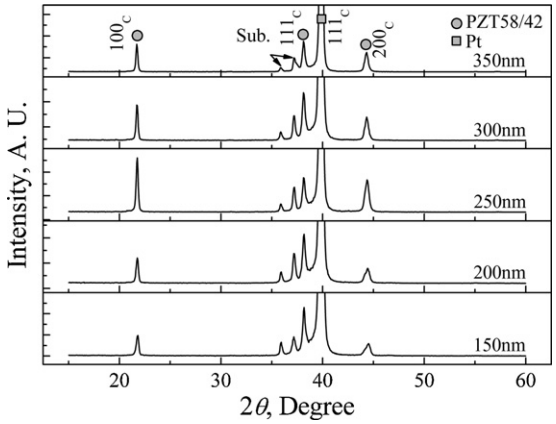

Fig. 3. θ–2θ scan XRD curves for PZT 58/42 films at $\psi = 0^\circ$.

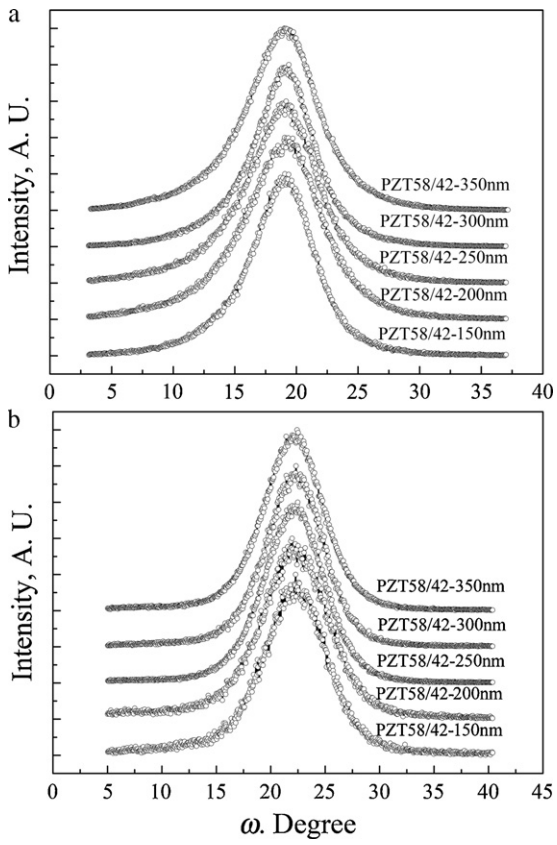

Fig. 4. ω-scan XRD curves for $1\,1\,1_C$ diffraction (a) and for $2\,0\,0_C$ diffraction (b) for PZT58/42 films with different thickness.

with the same orientation. Furthermore, the texture is symmetrical to the film normal direction. Consequently, the diffraction peaks for (*hkl*)-oriented grains can be obtained through tilting the film.

Because the films have the mixed textures of $(1\,0\,0)_C$ and $(1\,1\,1)_C$, the phase structures of (1 0 0)- and (1 1 1)-oriented grains should be studied separately. For (1 0 0)-oriented grains, the high-intensity peaks correspond to $2\,0\,0_C$ at $\psi = 0^\circ$ and $1\,1\,1_C$ at $\psi = 55^\circ$ because the interplanar angle between $\{1\,0\,0\}_C$ and $\{1\,1\,1\}_C$ is about 55° (see Fig. 5a). Similarly, for (1 1 1)-oriented grains, the high-intensity peaks correspond to $1\,1\,1_C$ at $\psi = 0^\circ$ and 200_C at $\psi = 55^\circ$ (see Fig. 5b). Because the diffraction peak features of $2\,0\,0_C$ and $1\,1\,1_C$ are very different among T, M and R phases, the phase types of PZT films in current work can be analyzed in comparison with the results of previous literatures [16,17,24].

3.3. Phase type of (1 0 0)-oriented grains

Fig. 6 shows the XRD curves for (1 0 0)-oriented grains of PZT58/42 films, which demonstrates that all diffraction peaks are asymmetrical. Each diffraction peak in Fig. 6 for PZT58/42 films is composed of at least two peaks. Especially when the film thickness is less than 250 nm, the peak is more obviously separated into at least two peaks. It was found that the T phase was seldom observed in PZT58/42 at room temperature [13,16,25]. Thus, the phase in the current PZT58/42 thin films may be R phase, M phase or R + M phases. $2\,0\,0_C$ diffraction peak of R phase should be single. But $2\,0\,0_C$ diffraction peak of M phase is composed of two peaks: $\{2\,0\,0\}_C$ and $\{0\,0\,2\}_C$, and their intensities quite differ due to the different multiplicity factors. For conventional XRD equipments, the $\{2\,0\,0\}_C$ and $\{0\,0\,2\}_C$ peaks of M phase have a partial overlap because of small difference in interplanar spacing. That is the reason why the

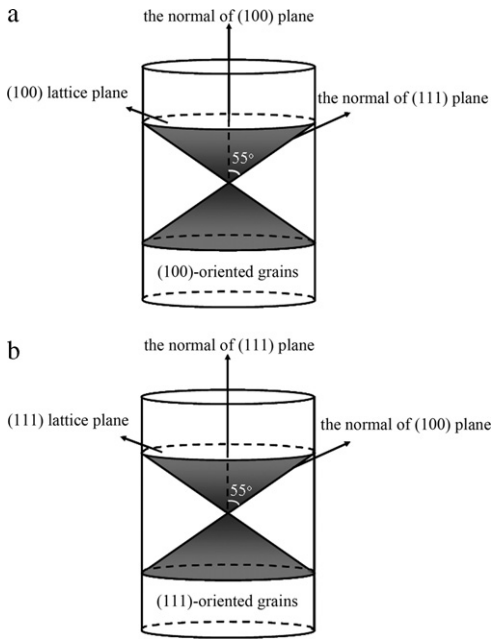

Fig. 5. $(1\,1\,1)_C$ normal direction distribution for ideal (1 0 0) texture (a) and $(1\,0\,0)_C$ normal direction distribution for ideal (1 1 1) texture (b).

$2\,0\,0_C$ peak of M phase is asymmetrical. As seen from Fig. 6(a), the $2\,0\,0_C$ diffraction peaks are asymmetrical, which indicates that the phase composition of (1 0 0)-oriented grains is not pure R phase.

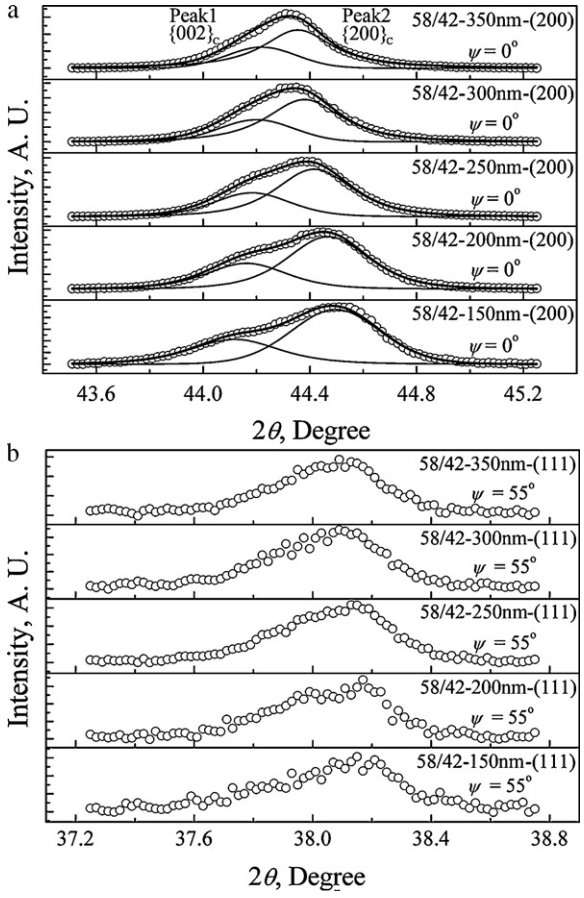

Fig. 6. Comparison of $2\,0\,0_C$ at $\psi = 0^\circ$ (a) and $1\,1\,1_C$ at $\psi = 55^\circ$ (b) XRD curves for (1 0 0)-oriented grains of PZT58/42 thin films with different film thickness.

$2\,0\,0_C$ diffraction peaks were fitted by Person VII function, and the fitting curves are also shown in Fig. 6(a). The intensity of peak 2 is about two times that of the peak 1 at low angle. As for M_A and M_C phases, the $\{0\,0\,2\}_C$ diffraction angle is lower than $\{2\,0\,0\}_C$ diffraction angle because interplanar spacing of $\{0\,0\,2\}_C$ plane is larger than that of $\{2\,0\,0\}_C$ plane. In addition, the multiplicity factor of $\{2\,0\,0\}_C$ plane is about two times that of $\{0\,0\,2\}_C$ plane. The peak shape of $2\,0\,0_C$ diffraction at $\psi = 0^\circ$ is similar to that of $2\,0\,0_C$ diffractions of M_A or M_C phases.

Fig. 6(b) shows the $1\,1\,1_C$ diffractions of (1 0 0)-oriented grains of PZT58/42 films. $1\,1\,1_C$ diffraction is composed of three diffraction peaks for M_A and M_C phases, but these three peaks are hardly separated by conventional XRD equipment. The peak shape of $1\,1\,1_{\mathbf{C}}$ diffraction for M_A or M_C phase was estimated on the basis of the previous researches [16,17] and the multiplicity factors. The peak shapes of $1\,1\,1_C$ diffractions given in Fig. 6(b) are consistent with those of M_A and M_C phases.

The above analysis of peak shapes of $2\,0\,0_C$ diffractions at $\psi = 0^\circ$ and $1\,1\,1_C$ diffractions at $\psi = 55^\circ$ suggests that the (1 0 0)-oriented grains in all films mainly contain M phase. Even though R phase existed in the films, its contents should be very little. The reason is attributed to two aspects. On one hand, if the lattice constants of R phase are quite different from those of M phase, the 2 0 0c diffraction peak should include three separate peaks. Among these three peaks, two of them belong to M_A or M_C phase, and the third one belongs to R phase. However, the actual results in Fig. 6(a) tell us that the $2\,0\,0_{\mathbf{C}}$ diffraction does not exhibits characteristic of three peaks but obvious characteristic of two peaks. On the other hand, if R phase and M phase have the close lattice constants, the relative intensity ratio of peak 2 over peak 1 should deviate from 2. However, the relative intensity ratio of peak 2 over peak 1 fitted by Person VII function is almost 2. These two points lead to the conclusion that the content of R phase is ignorant.

However, it is very hard to identify whether the phase composition of (1 0 0)-oriented grains is M_A phase or M_C phase because the diffraction peak symmetry of M_A and M_C phases is similar. But the R phase is easy to transform to M_A phase under the condition of the residual stress [26]. So the phase of (1 0 0)-oriented grains may be identified as M_A phase.

Fig. 7(a) shows the FWHM of $2\,0\,0_C$ diffraction peaks of (1 0 0)-oriented grains. The FWHM of $2\,0\,0_C$ decreases as the film thickens, which means that $\{2\,0\,0\}_C$ and $\{0\,0\,2\}_C$ peak positions become closer as the film become thicker. The ratio of $d_{\{002\}_C}/d_{\{200\}_C}$ is shown in Fig. 7(b). As the film thickness increases, the $d_{\{002\}_C}/d_{\{200\}_C}$ ratio in (1 0 0)-oriented grains decreases till approaches 1, which means these two peaks are gradually close to each other. These results suggest that the lattice constants of M_A phase are changeable as the film thickness varies. The details will be discussed in section 4.

3.4. Phase type of (1 1 1)-oriented grains

The $2\,0\,0_C$ diffractions at $\psi = 55^\circ$ and $1\,1\,1_C$ diffractions at $\psi = 0^\circ$ were measured to analyze the phase type of (1 1 1)-oriented grains, and the results are presented in Fig. 8. We used the same method to analyze the (1 1 1)-oriented grains.

The $2\,0\,0_C$ diffraction peaks at $\psi = 55^\circ$ are shown in Fig. 8(a). However, the peak symmetry is opposite to that in Fig. 6(a). Obviously this peak can also be separated into two peaks, and the relative intensity ratio of peak 3 over peak 4 is almost 2, which demonstrates that M_B phase exists in (1 1 1)-oriented grains. For M_B phase, the interplanar spacing of $\{2\,0\,0\}_C$ is larger than that of $\{0\,0\,2\}_C$, and the multiplicity factor of $\{2\,0\,0\}_C$ is two times that of $\{0\,0\,2\}_C$. This gives rise to the result that the intensity of peak 3 is about two times that of peak 4. Therefore, the peak symmetry in Fig. 8(a) is opposite to that in Fig. 6(a).

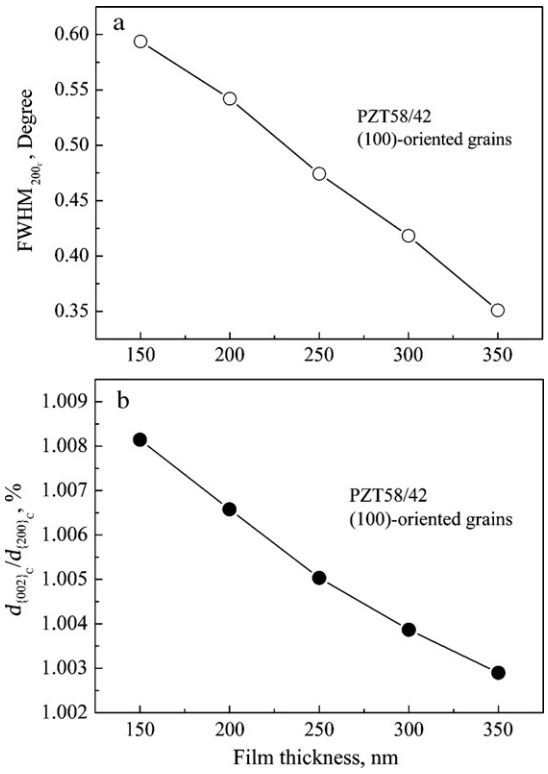

Fig. 7. FWHM of $2\,0\,0_C$ diffraction at $\psi = 0^\circ$ (a) and the ratio of $d_{\{002\}_C}/d_{\{200\}_C}$ (b) of (1 0 0)-oriented grains for PZT58/42 films with different thickness.

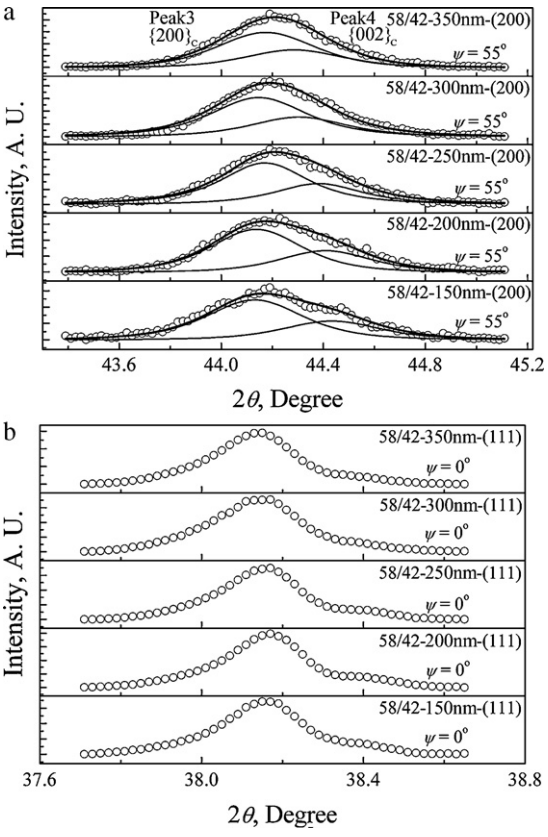

Fig. 8. Comparison of $2\,0\,0_C$ at $\psi = 55^\circ$ (a) and $1\,1\,1_C$ at $\psi = 0^\circ$ (b) XRD curves for (1 1 1)-oriented grains of PZT58/42 thin films with different thickness.

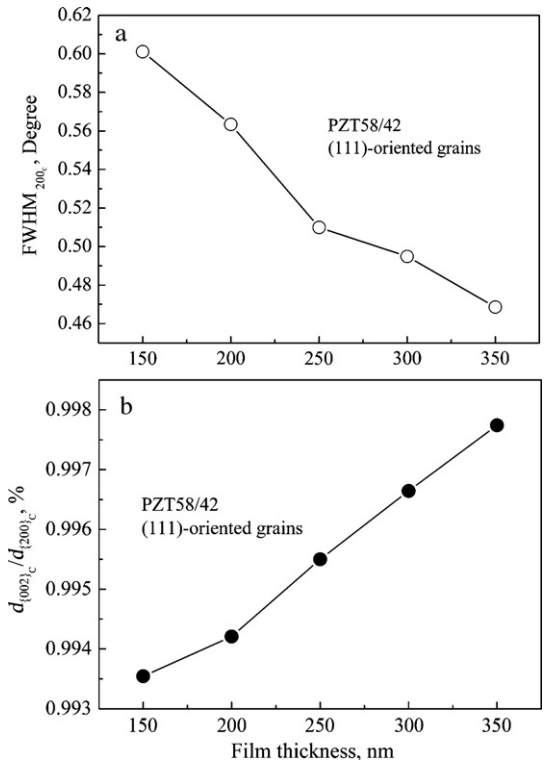

Fig. 9. FWHM of $2\,0\,0_C$ diffraction at $\psi = 55^\circ$ (a) and the ratio of $d_{\{002\}_C}/d_{\{200\}_C}$ (b) of (1 1 1)-oriented grains for PZT58/42 films with different thickness.

Similarly, the symmetry of $1\,1\,1_C$ diffraction peak of M_B phase should also be the opposite to that of M_A phase peak, because the lattice constant *c* is shorter than *a* and *b* for M_B phase when using the pseudocubic coordinate system. At the same time, the FWHM of $2\,0\,0_C$ at $\psi = 55^\circ$ for (1 1 1)-oriented grains decreases gradually as the film thickens, as shown in Fig. 9(a). This implies that the interplanar spacings of the $\{2\,0\,0\}_C$ and the $\{0\,0\,2\}_C$ planes become closer with the film thickness increasing. The ratio of $d_{\{002\}_C}/d_{\{200\}_C}$ is shown in Fig. 9(b). It is also found that the ratio gradually approaches to 1 with the film thickness increasing. This suggests that the phase type in the infinitely thick film (i.e. like stress-free ceramics) is R phase. This result is consistent with the previous reports where bulk PZT58/42 was considered as R phase. [4,13]

3.5. Raman spectra

In order to further confirm the phase composition of PZT58/42 films, Raman spectrum tests were conducted, and the results are shown in Fig. 10. It is seen that all the films exhibit the similar profiles, which means that all the films have the similar phase composition. Moreover, the Raman spectra of the PZT58/42 films exhibit the similar characteristics to that of PZT53/47 with M phase [27]. This Raman evidence is not contradictory to M phase in the PZT58/42 films.

4. Discussion

The phase composition of PZT58/42 falling in the R phase region of the phase diagram was reported by Noheda et al. [13] (see Fig. 1). But in this study, the phase composition of PZT 58/42 films with different film thickness is M phase, which suggests that the phase transition from R phase to M phase took place due to the residual stress in thin films. Meanwhile, (1 0 0)- and (1 1 1)-oriented grains are of M_A and M_B phases, respectively, which may be caused by the following reasons. On the one hand, the lattice mismatch between

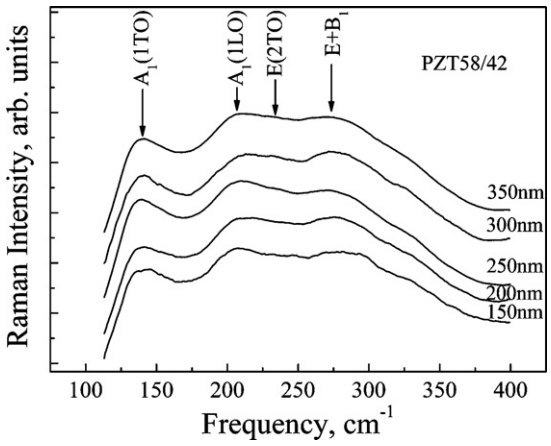

Fig. 10. Raman spectra of PZT58/42 thin films with different thickness.

(1 0 0)-oriented grains and (1 1 1)-oriented Pt substrate is different from that between (1 1 1)-oriented grains and (1 1 1)-oriented Pt substrate. [28], and the residual stress state in (1 0 0)-oriented grains is different from that in (1 1 1)-oriented grains as well [29]. On the other hand, because of the different residual stress components of different-orientation grains in crystalline coordinates, Pb ion displacement direction for different-orientation grains induced by residual stress is different in perovskite unit cell, which leads to the difference in the symmetry of M phase.

Generally speaking, the residual stress decreases with the film thickness increasing [30]. If the diffraction peak displacements are only caused by residual stress, the peak displacement directions for all diffractions should be the same. However, as shown in Figs. 6(a) and 8(a), with the film thickness increasing, the displacement directions of $\{2\,0\,0\}_C$ and $\{0\,0\,2\}_C$ diffraction peaks are converse and the two peaks approach to each other gradually, independent of (1 0 0)- or (1 1 1)-oriented grains. These results indicate that the diffraction peak displacements result from the change of lattice constants of M phase due to the residual stress changing in films. Accordingly, as shown in Figs. 7(b) and 9(b), $d_{\{002\}_C}/d_{\{200\}_C}$ ratios approach 1 gradually with the film thickness increasing. This means that the displacement of Pb ion becomes smaller and smaller, and the lattice constants of M phase are gradually close to those of strain-free R phase.

The change of lattice constants of M phase means that the spontaneous polarization direction of M phase is variable. Fig. 11 shows the rotation mechanism of spontaneous polarization direction of M phase with the film thickness increasing. The spontaneous polarization direction of M phase in $(x, x, 0)_C$ plane rotates to that of R phase with the residual stress decreasing. The above results are consistent with the previous studies where the origin of the giant piezoelectric response of PZT thin film is considered as the result of the rotation of spontaneous polarization direction of M phase [10].

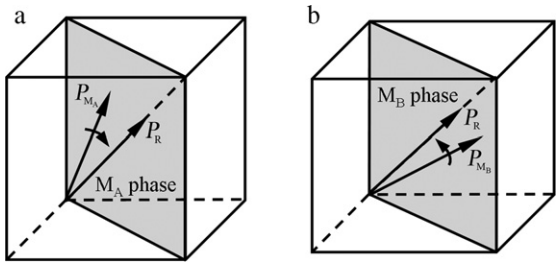

Fig. 11. Schematic diagram of the spontaneous polarization direction rotation of M_A and M_B phases with residual stress decreasing.

According to above discussion, we can conclude that the lattice constants of M phase are very sensitive to the state and magnitude of residual stress. In previous literatures, the M phase lattice constants quite differ (see Table 1). We think that this may be resulted from different residual stress in samples. Stress-free samples are hardly prepared because large residual stress may be induced by non-180° domain walls. Consequently, obtaining the unified lattice constants of M phase is very hard.

5. Conclusion

PZT58/42 films with the composition in the R phase region are found to have mixed textures of (1 0 0) and (1 1 1). The phase composition of the PZT films was confirmed as M phase, but the phase composition of different-orientation grains is different. The (1 0 0)-oriented grains mainly conclude M_A phase and (1 1 1)-oriented grains conclude M_B phase. In addition, the $d_{\{002\}_C}/d_{\{200\}_C}$ ratio of M phase approaches 1 gradually with the film thickness increasing, which implies the variation of the spontaneous polarization direction of M phase.

References

[1] M. Ahart, M. Somayazulu, R.E. Cohen, P. Ganesh, P. Dera, H. Mao, R.J. Hemley, Y. Ren, P. Liermann, Z.G. Wu, Nature 451 (2008) 545.
[2] A. Nourmohammadi, M.A. Bahrevar, M. Hietschold, J. Alloys Compd. 473 (2009) 467–472.
[3] Y.H. Yu, M.O. Lai, L. Lu, P. Yang, J. Alloys Compd. 449 (2008) 56–59.
[4] B. Jaffe, W.R. Cook, H. Jaffe, Piezoelectric Ceramics, Academic, London, 1971, p.136.
[5] B. Noheda, D.E. Cox, G. Shirane, J.A. Gonzalo, L.E. Cross, S.-E. Park, Appl. Phys. Lett. 74 (1999) 2059–2061.
[6] V.Y. Topolov, A.V. Turik, J. Phys.: Condens. Matter 13 (2001) L771–L775.
[7] J.Z. Xiao, X.Y. Zhang, P.P. Zhu, W.X. Huang, Q.X. Yuan, Solid State Commun. 148 (2008) 109–112.
[8] Z.G. Wu, H. Krakauer, Phys. Rev. B 68 (2003) 014112.
[9] G. Shabbir, S. Kojima, C. Feng, J. Appl. Phys. 100 (2006) 064107.
[10] R. Guo, L.E. Cross, S.-E. Park, B. Noheda, D.E. Cox, G. Shirane, Phys. Rev. Lett. 84 (2000) 5423–5426.
[11] B. Noheda, J.A. Gonzalo, L.E. Cross, R. Guo, S.-E. Park, D.E. Cox, G. Shirane, Phys. Rev. B 61 (2000) 8687–8695.
[12] D. Damjanovic, Appl. Phys. Lett. 97 (2010) 062906.
[13] B. Noheda, D.E. Cox, G. Shirane, R. Guo, B. Jones, L.E. Cross, Phys. Rev. B 63 (2000) 014103.
[14] H. Yokota, N. Zhang, A.E. Taylor, P.A. Thomas, A.M. Glazer, Phys. Rev. B 80 (2009) 104109.
[15] D. Pandey, A.K. Singh, S. Baik, Acta Crystallogr., Sect. A: Found. Crystallogr. A64 (2008) 192–203.
[16] A.K. Singh, D. Pandey, S. Yoon, S. Baik, N. Shin, Appl. Phys. Lett. 91 (2007) 192904.
[17] R. Ragini, S.K. Ranjan, D. Mishra, Pandey, J. Appl. Phys. 92 (2002) 3266–3274.
[18] J. Frantti, S. Ivnov, S. Eriksson, H. Rundlöf, V. Lantto, J. Lappalainen, M. Kakihana, Phys. Rev. B 66 (2002) 064108.
[19] J. Frantti, J. Lappalainen, S. Eriksson, V. Lantto, S. Nishio, K. Kakihana, S. Ivanov, H. Rudlöf, Jpn. J. Appl. Phys. 39 (2000) 5697–5703.
[20] E.B. Araújo, E.C. Lima, J.D.S. Guerra, A.O. dos Santos, L.P. Cardoso, M.U. Kleinke, J. Phys.: Condens. Matter 20 (2008) 415203.
[21] J. Frantti, S. Eriksson, S. Hull, V. Lantto, H. Rundlöf, M. Kakihana, J. Phys.: Condens. Matter 15 (2003) 6031–6041.
[22] K.A. Schönau, L.A. Schmitt, M. Knapp, H. Fuess, R.-A. Eichel, H. Kungl, M.J. Hoffmann, Phys. Rev. B 75 (2007) 184117.
[23] W.D. Fei, C.Q. Liu, M.H. Ding, W.L. Li, L.D. Wang, Rev. Sci. Instrum. 80 (2009) 093903.
[24] Y.U. Wang, Phys. Rev. B 76 (2007) 024108.
[25] Z.J. Wang, Y. Aoki, L.J. Yan, H. Kokawa, R. Maeda, J. Crystal Growth 267 (2004) 92–99.
[26] H.W. Jang, S.H. Baek, D. Ortiz, C.M. Folkman, R.R. Das, Y.H. Chu, P. Shafer, J.X. Zhang, S. Choudhury, V. Vaithyanathan, Y.B. Chen, D.A. Felker, M.D. Biegalski, M.S. Rzchowski, X.Q. Pan, D.G. Schlom, L.Q. Chen, R. Ramesh, C.B. Eom, Phys. Rev. Lett. 101 (2008) 107602.
[27] A.G. Souza Filho, K.C.V. Lima, A.P. Ayala, I. Guedes, P.T.C. Freire, F.F.A. Melo, J. Mendes Filho, E.B. Araújo, J.A. Eiras, Phys. Rev. B 66 (2002) 132107.
[28] Z. Huang, Q. Zhang, R.W. Whatmore, J. Appl. Phys. 85 (1999) 7355–7361.
[29] J.N. Wang, W.L. Li, B. Feng, C.Q. Liu, X.L. Li, Q. Sun, W.D. Fei, J. Alloys Compd. 506 (2010) 167–171.
[30] Y. Sakamaki, H. Fukazawa, N. Wakiya, H. Suzuki, K. Shinozaki, T. Ohno, M. Kosec, Jpn. J. Appl. Phys. 46 (2007) 6925–6928.